Front. Optoelectron. 2018, 11(3): 285–290
https://doi.org/10.1007/s12200-018-0758-4

RESEARCH ARTICLE

ZnO/Nb_2O_5 core/shell nanorod array photoanode for dye-sensitized solar cells

Xiaoyan HU, Heng WANG (✉)

College of New Energy and Electronic Engineering, Yancheng Teachers University, Yancheng 224002, China

Abstract In this paper, ZnO/Nb_2O_5 core/shell nanorod arrays were synthesized and used as photoanodes for dye-sensitized solar cells (DSSCs). We first synthesized ZnO nanorod array on fluorine-doped tin oxide (FTO) glasses by a hydrothermal method, and then ZnO/Nb_2O_5 core/shell nanorod array was directly obtained via solvothermal reaction in $NbCl_5$ solution. The scanning electron microscope (SEM) and transmission electron microscope (TEM) images revealed that the ZnO nanorods were uniformly wrapped by Nb_2O_5 shell layers with a thickness of 30–40 nm. Photovoltaic characterization showed that the device based on ZnO/Nb_2O_5 core/shell nanorod photoanode exhibited an improved efficiency of 1.995%, which was much higher than the efficiency of 0.856% for the DSSC based on bare ZnO nanorod photoanode. This proved that the photovoltaic performance of ZnO nanorods could be improved by wrapping with Nb_2O_5 shells.

Keywords ZnO, Nb_2O_5, core/shell nanorods, solvothermal, dye-sensitized solar cell (DSSC)

1 Introduction

As a promising alternative to conventional silicon-based solar cell, dye-sensitized solar cells (DSSCs) have attracted considerable attention in the last two decades, because of their low manufacturing costs and relatively high energy-conversion efficiencies [1–4]. In DSSC components, the photoanode is a key part that plays an essential role in determining the dye loading and electron transportation, and hence the photon to electron conversion efficiency. To realize highly efficient DSSC, a nanostructured photoanode should possess several favorable intrinsic characteristics, such as large surface area to permit high dye loading, direct electron transport pathways for long electron diffusion lengths, and compatible energy levels to achieve high electron injection efficiency and high voltage. It is therefore highly desirable to develop a photoanode that meets the above requirements.

There have been many efforts to develop efficient photoanode materials such as TiO_2, ZnO, SnO_2, Nb_2O_5, and other composites. So far, TiO_2 has been widely investigated as a photoanode material for DSSCs. With a band gap similar to that of TiO_2, ZnO is another alternative photoanode material, which has attracted much attention due to its high mobility of about 115–155 $cm^2 \cdot V^{-1} \cdot s^{-1}$, which is much higher than that of TiO_2 (10^{-5} $cm^2 \cdot V^{-1} \cdot s^{-1}$) [5,6]. Among the various morphologies, one-dimensional (1D) nanostructures such as nanorods, nanotubes, and nanowires, which can offer more superior electron transport pathways, have been attracting increasing attention. However, the power conversion efficiencies of DSSCs based on ZnO 1D nanostructures are still at relatively low levels, because of the insufficient internal surface area.

To overcome this shortcoming, it is necessary to design a novel core/shell photoanode by applying metal oxide shells such as SiO_2 [7], ZrO_2 [8], Nb_2O_5 [9–12], and Al_2O_3 [13] to the core nanostructures. The metal oxide shells synthesized on core nanostructures could increase the specific area of the electrode for dye loading, thereby enhancing the photocurrent density. Moreover, the layer formed by coating with these materials act as an energy barrier that decreases the electron recombination losses, shifts the conduction band downward, which increases the electron injection, and enhances the injection efficiency.

Nb_2O_5 is a promising metal oxide because it supports good N719 dye loading due to its basic character [14–17], and its conduction band level is more negative than that of TiO_2 [18,19]. Here, we applied a Nb_2O_5 coating on ZnO nanorod to obtain ZnO/Nb_2O_5 core/shell nanorod arrays, which were used as the photoanodes in DSSCs. The results showed that improved efficiencies of 1.609% and 1.995% were obtained for DSSCs based on ZnO/Nb_2O_5 core/shell

Received September 26, 2017; accepted December 8, 2017

E-mail: wangheng8463@163.com

nanorod synthesized in-low concentration $NbCl_5$ solution and in high-concentration $NbCl_5$ solution, respectively, compared with the efficiency of 0.856% for the DSSC based on bare ZnO nanorod photoanode.

2 Experimental

2.1 Synthesis of ZnO nanorod arrays

The ZnO seed layer on fluorine-doped tin oxide (FTO) glasses was prepared using a previously published procedure [20]. Then, 0.455 g $Zn(NO_3)_2 \cdot 6H_2O$ and 0.555 g NH_4F were dissolved into 50 mL deionized water. After that, $NH_3 \cdot H_2O$ was dropped into the above solution while stirring. In this process, the clear solution turned turbid when $NH_3 \cdot H_2O$ was first dropped into the solution, and then gradually it turned clear with continued stirring. Subsequently, the prepared ZnO seed layer on FTO glass (with the FTO layer facing downwards) was placed into a Teflon-lined autoclave, which contained the above solution, and was then sealed. Finally, the Teflon-lined autoclave was heated at 70°C for 8 h to obtain ZnO nanorod arrays.

2.2 Synthesis of ZnO/Nb_2O_5 core/shell nanorod arrays

Figure 1 shows the process of growing ZnO/Nb_2O_5 core/shell nanorod arrays on FTO glass. First, 0.135 and 0.270 g $NbCl_5$ were dissolved into 50 mL anhydrous ethanol. After that, the obtained ZnO nanorod arrays were placed into the two Teflon-lined autoclaves, each containing one of the above two $NbCl_5$ solutions. Then, the Teflon-lined autoclaves were heated at 180°C for 24 h to obtain ZnO/Nb_2O_5 core/shell nanorod arrays with ZnO/Nb_2O_5(1) for 0.135 g $NbCl_5$ and ZnO/Nb_2O_5(2) for 0.270 g $NbCl_5$. Finally, the ZnO/Nb_2O_5 core/shell nanorod arrays were sintered at 500°C in air for 1 h.

2.3 Fabrication of DSSCs based on ZnO/Nb_2O_5 core/shell nanorod arrays

The ZnO/Nb_2O_5 core/shell nanorod arrays were dipped in a dye solution containing 0.5 mM[1)] N719 (Dyesol) dye for 24 h. Then, the ZnO/Nb_2O_5 electrode was scrapped to obtain an active area of 25 mm^2. The counter electrode was prepared by coating a 0.6 mM $H_2PtCl_6 \cdot 6H_2O$ solution in anhydrous ethanol onto the FTO substrate. After that, the ZnO/Nb_2O_5 electrode was assembled with the counter electrode by clamping a 25 μm thick polymeric film (Surlyn, DuPont). Then, an electrolyte solution was injected into the gap between the ZnO/Nb_2O_5 electrode and the counter electrode. The electrolyte solution contained 0.05 M LiI (Sigma-Aldrich), 0.03 M I_2 (Aldrich), and 0.5 M 4-tert-butylpyridine (Aldrich) in a solution containing acetonitrile (Aldrich). Finally, the injecting hole was sealed with an adhesive tape to obtain the completed device.

2.4 Characterization

A scanning electron microscope (SEM, Quanta200, FEI,

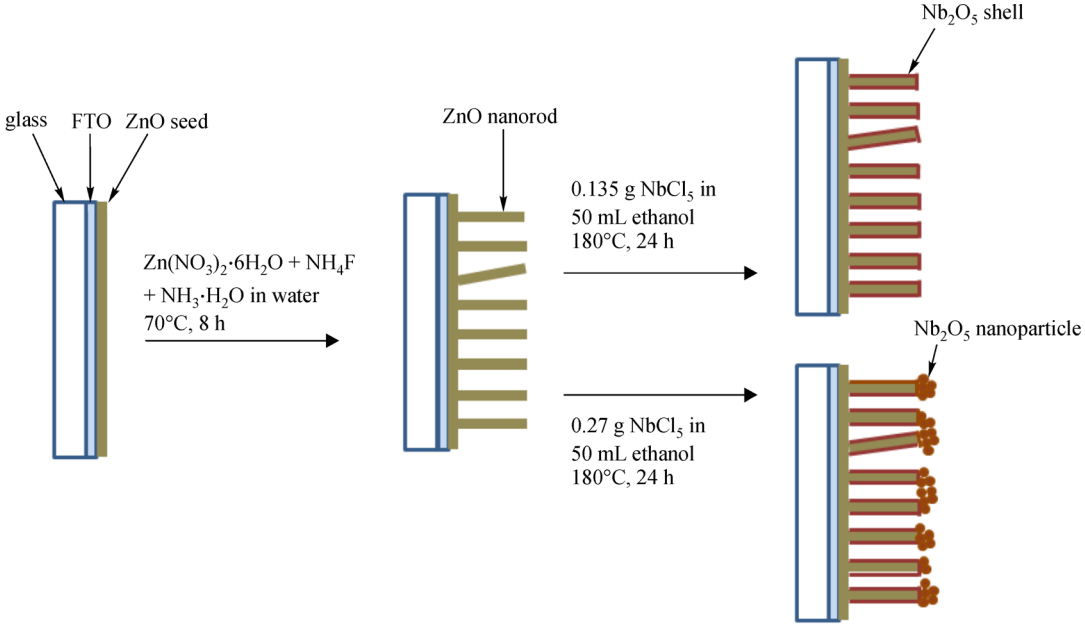

Fig. 1 Schematic diagram of the ZnO/Nb_2O_5 core/shell nanorod arrays

1) 1 mM = 1 mmol/L

Netherlands) and a transmission electron microscope (TEM, JEOL TEM-2010) were used to measure the structure and morphology of the nanomaterials. The current–voltage characterization was performed using a Keithley 2400 source meter under simulated AM 1.5 sunlight illumination (100 $mW \cdot cm^{-2}$) provided by an Oriel solar simulator (Model 9119X, Newport Co.). The illuminated active area of the photovoltaic measurements was 0.16 cm^2. The electrochemical impedance spectra (EIS) of the devices were tested at -0.6 V for the range from 1 MHz to 1 Hz, with an advanced electrochemical system (PAR2273) under dark conditions.

3 Results and discussion

3.1 Structural and morphological characterization of ZnO/ Nb_2O_5 core/shell nanorod

Figures 2(a) and 2(b) show the top-view and cross-view SEM images of the ZnO nanorod arrays, respectively. Figure 2(a) reveals that the top of the nanorods is uniform. From the tilted-view SEM image, we can clearly see that the high-density ZnO nanorods grew vertically on the FTO substrate. Their length is about 5 μm. After the coating of the Nb_2O_5 shell, the core-shell structure was investigated by SEM. Figure 2(c) shows the top-view SEM image of the ZnO/ Nb_2O_5 core-shell nanorod film. It clearly reveals that the diameter of the core-shell nanorod increased and its surface became rough. The corresponding tilted-view SEM image shows that the core-shell structure has a similar shape as that of the ZnO nanorod shown in Fig. 2(d). To investigate the coating of Nb_2O_5, the samples were synthesized in a low-concentration $NbCl_5$ solution (0.135 g $NbCl_5$) and a higher-concentration $NbCl_5$ solution (0.270 g $NbCl_5$). The results are shown in Fig. 3. By comparison, we could find that upon increasing the concentration of $NbCl_5$, the ZnO nanorods became rougher on the side surface and were fully covered with Nb_2O_5 nanoparticles on the top. This shows that a high concentration of $NbCl_5$ could facilitate significantly more growth of Nb_2O_5 on the top of the nanorod than on its side.

In the TEM image (Fig. 4(a)), obvious differences in terms of the contrast between the center and fringe parts of each individual rod-like structure are observed, which indicates that the rod-like structures are core-shell structures with core diameters of 150–200 nm and shell thicknesses of 30–40 nm. The corresponding sellected area electron diffraction (SAED) pattern obtained from the circled area in Fig. 4(a) is shown in Fig. 4(b). We can see single crystal diffraction spots in Fig. 4(b), corresponding to ZnO (103) and (203). In addition, Fig. 4(b) also shows an amorphous diffraction pattern, which is indicated by the dotted line. We measured the radius of the amorphous diffraction ring, and the spacing between the crystal planes ranged from 0.39 to 0.28 nm, which was consistent with the strong peak position of JCPDS (320711) Nb_2O_5. Therefore, we inferred that the amorphous diffraction ring was from the amorphous Nb_2O_5 wrapped on the surface of ZnO.

3.2 Characterization of photovoltaic performances for DSSCs

Figure 5 shows the optical absorption spectra of the ZnO

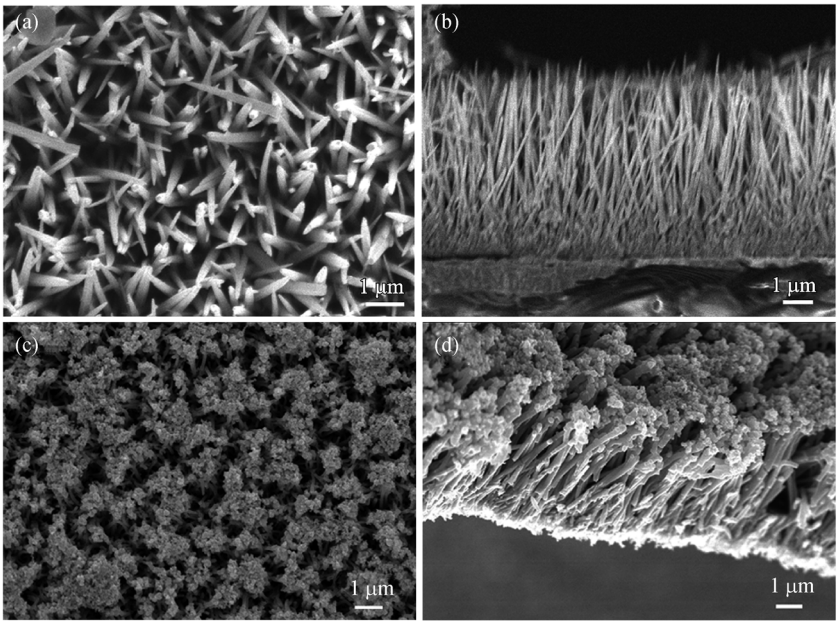

Fig. 2 Top-view (a) and tilted-view SEM images (b) of bare ZnO nanorod arrays. The top-view (c) and tilted-view SEM images (d) of ZnO/Nb_2O_5 core/shell nanorod arrays obtained in high concentration $NbCl_5$ solution (0.270 g $NbCl_5$)

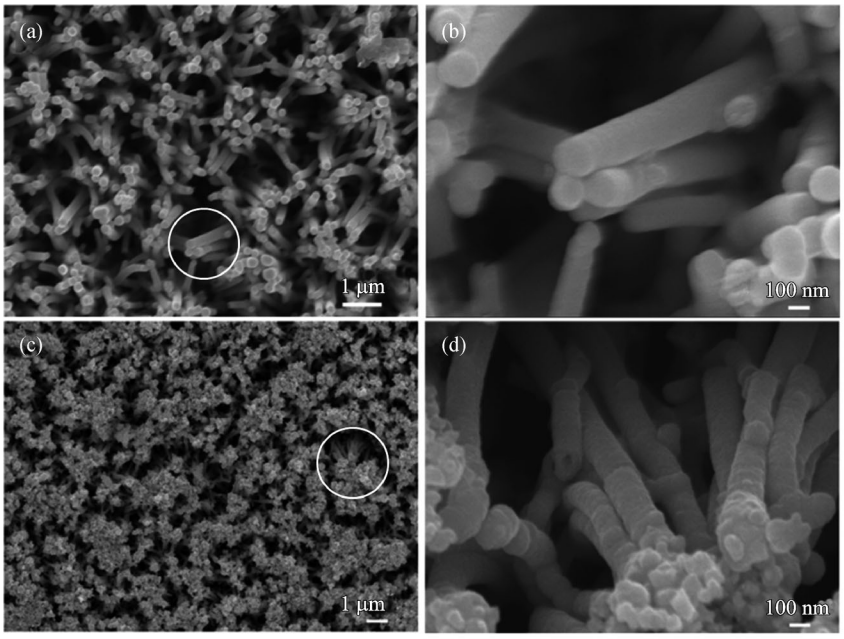

Fig. 3 Top-view SEM images of ZnO/Nb_2O_5 core/shell nanorod arrays synthesized in low concentration $NbCl_5$ solution (0.135 g $NbCl_5$): (a) low and (b) high magnification. The top-view SEM images of ZnO/Nb_2O_5 core/shell nanorod arrays synthesized in high concentration $NbCl_5$ solution (0.270 g $NbCl_5$): (c) low and (d) high magnification

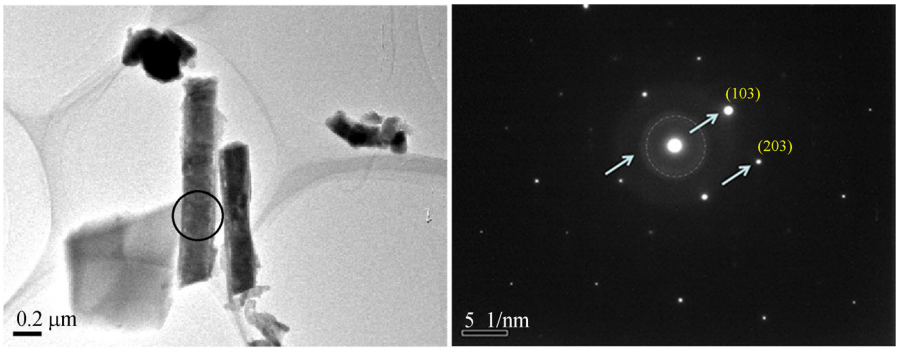

Fig. 4 (a) TEM image of ZnO/Nb_2O_5 core/shell nanorod and (b) the corresponding SAED pattern obtained from the circle area in Fig. 4(a)

and ZnO/Nb_2O_5 nanorod films. For the bare ZnO nanorod film, the onset of the band gap transition is at ~420 nm. The presence of Nb_2O_5 shell increases another adsorption edge at ~370 nm relative to Nb_2O_5. Compared with the ZnO nanorod arrays, the coating of the Nb_2O_5 moved the onset of absorption to a lower wavelength, and the light absorption intensity was enhanced. The larger band gap of Nb_2O_5 semiconductor is related to the more negative conduction band potential and the larger open-circuit photovoltage of the Nb_2O_5 cell. This result is consistent with the following photovoltaic performances.

The photocurrent density-voltage curves of DSSCs based on the photoanodes of bare ZnO nanorods, ZnO/Nb_2O_5(1) core/shell nanorod (0.135 g $NbCl_5$), and ZnO/Nb_2O_5(2) core/shell nanorod (0.270 g $NbCl_5$) are shown in Fig. 6. The photovoltaic performances of the three devices are listed in Table 1. The device based on the photoanode of bare ZnO nanorods showed poor performances with short-circuit current density (J_{sc}), open-circuit voltage (V_{oc}), fill factor (*FF*), and power conversion efficiency (PCE) of 4.46 $mA \cdot cm^{-2}$, 537 mV, 0.357, and 0.856%, respectively. This efficiency was similar to the efficiencies of DSSCs based on bare ZnO nanorod arrays reported by other groups [21,22]. The device based on ZnO/Nb_2O_5(1) core/shell nanorod exhibited improved performances with J_{sc}, V_{oc}, *FF*, and PCE of 5.52 $mA \cdot cm^{-2}$, 569 mV, 0.512, and 1.609%, respectively. The increased J_{sc} is mainly attributed to the increased surface area of ZnO/Nb_2O_5 core/

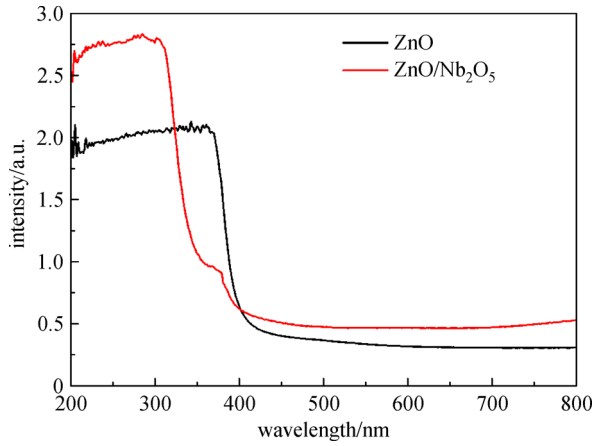

Fig. 5 Optical absorption spectra of ZnO and ZnO/Nb_2O_5 nanorod arrays

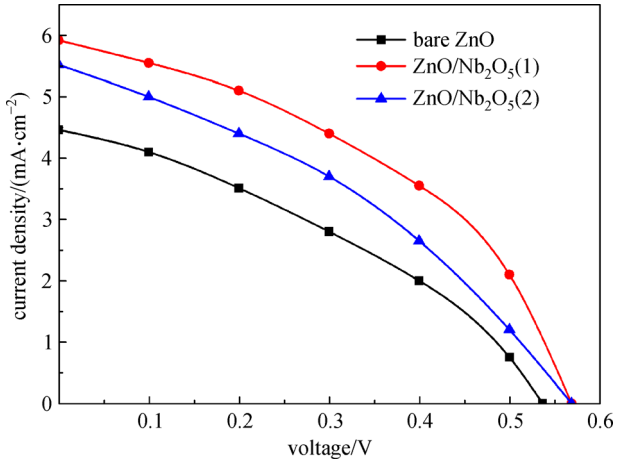

Fig. 6 Photocurrent density-voltage curves of DSSCs based on the photoanodes of bare ZnO nanorods, $ZnO/Nb_2O_5(1)$ core/shell nanorod (0.135 g $NbCl_5$) and $ZnO/Nb_2O_5(2)$ core/shell nanorod (0.270 g $NbCl_5$)

shell nanorod, which was caused by the small Nb_2O_5 nanoparticles wrapped on the ZnO nanorod. The increased V_{oc} is attributed to the fact that the Fermi level of ZnO/ Nb_2O_5 core/shell nanorod is higher than that of bare ZnO nanorod, since Nb_2O_5 has a higher conduction band than ZnO. This increases the V_{oc} value because the maximum V_{oc} of DSSC is mainly decided by the difference between the Fermi level of the photoanode and the redox potential of I^-/I_3^-. In addition to the increased J_{sc} and V_{oc}, the device based on $ZnO/Nb_2O_5(1)$ core/shell nanorod exhibited a higher *FF* of 0.512 than the device based on ZnO nanorod (0.357). This indicates that the Nb_2O_5 shell provided another charge-transporting channel other than the ZnO nanorod, resulting in decreased series resistance. As for the device based on $ZnO/Nb_2O_5(2)$ core/shell nanorod, the J_{sc}, *FF*, and PCE were further increased to 5.95 $mA \cdot cm^{-2}$, 0.592, and 1.995%, respectively. Compared with the ZnO/ $Nb_2O_5(1)$ core/shell nanorod, the $ZnO/Nb_2O_5(2)$ core/shell nanorod had a thicker diameter and had additional Nb_2O_5 particles on top of the nanorod. Such a core/shell nanorod structure makes the ZnO/Nb_2O_5 nanorod photoanode advantageous in the following two aspects. On the one hand, since the protons that are released from the dye molecules in the ethanolic solution dissolved ZnO to generate Zn^{2+}-dye aggregates, the structure of the ZnO crystals was easily destroyed after loading the Ru-complex dyes. However, after being coated with Nb_2O_5, the recombination was suppressed by passivating its centers on the ZnO nanostructure surface. On the other hand, the electrolyte was suppressed presumably due to the energy barrier formed at the ZnO/ Nb_2O_5 interface. Thus, J_{sc} and V_{oc} of the ZnO/ Nb_2O_5 nanorod photoanode are much higher than that of the bare ZnO photoanode.

4 Conclusions

In summary, ZnO/Nb_2O_5 core/shell nanorods were successfully developed by solvothermal synthesis and applied as photoanodes for DSSCs. ZnO nanorod core was first synthesized by a hydrothermal process, and then Nb_2O_5 shell was directly synthesized on the ZnO nanorod core by solvothermal reaction in $NbCl_5$ solution. SEM and TEM images revealed that the ZnO nanorods were uniformly wrapped by the Nb_2O_5 shell layers with a thickness of 30–40 nm. Photovoltaic characterization showed that improved efficiencies of 1.609% and 1.995% were obtained for DSSCs based on ZnO/Nb_2O_5 core/shell nanorod synthesized in low-concentration $NbCl_5$ solution and high-concentration $NbCl_5$ solution, respectively, compared with the efficiency of 0.856% for the DSSC based on bare ZnO nanorod photoanode. Our work offers a facile strategy to develop functional composite nanomaterials for photovoltaic devices.

Table 1 Photovoltaic performance of DSSCs based on photoanodes of ZnO nanorods, $ZnO/Nb_2O_5(1)$ nanorod and $ZnO/Nb_2O_5(2)$ nanorod under AM1.5 conditions 100 $mW \cdot cm^{-2}$. The length of three nanorods in the devices are all around 5 μm

photoanode	$J_{sc}/(mA \cdot cm^{-2})$	V_{oc}/mV	*FF*	PCE/%
ZnO	4.46	537	0.357	0.856%
$ZnO/Nb_2O_5(1)$	5.52	569	0.512	1.609%
$ZnO/Nb_2O_5(2)$	5.92	569	0.592	1.995%

Acknowledgements The authors acknowledge the financial support from the National Natural Science Foundation of China (Grant Nos. 11647073, 11547263) and the financial support from High Education Natural Science Research Project of Jiangsu Province (No. 15KJB430033).

References

1. O'Regan B, Grätzel M. A low-cost, high-efficiency solar cell based on dye-sensitized colloidal TiO_2 films. Nature, 1991, 353(6346): 737–740
2. Bach U, Lupo D, Comte P, Moser J E, Weissortel F, Salbeck J, Spreitzer H, Grätzel M. Solid-state dye-sensitized mesoporous TiO_2 solar cells with high photon-to-electron conversion efficiencies. Nature, 1998, 395(6702): 583–585
3. Shang Y, Hao S, Yang C, Chen G. Enhancing solar cell efficiency using photon upconversion materials. Nanomaterials (Basel, Switzerland), 2015, 5(4): 1782–1809
4. Hao S, Shang Y, Li D, Ågren H, Yang C, Chen G. Enhancing dye-sensitized solar cell efficiency through broadband near-infrared upconverting nanoparticles. Nanoscale, 2017, 9(20): 6711–6715
5. Prabakar K, Son M, Kim W Y, Kim H. TiO_2 thin film encapsulated ZnO nanorod and nanoflower dye sensitized solar cells. Materials Chemistry and Physics, 2011, 125(1–2): 12–14
6. Chandiran A K, Abdi-Jalebi M, Nazeeruddin M K, Grätzel M. Analysis of electron transfer properties of ZnO and TiO_2 photoanodes for dye-sensitized solar cells. ACS Nano, 2014, 8(3): 2261–2268
7. Palomares E, Clifford J N, Haque S A, Lutz T, Durrant J R. Control of charge recombination dynamics in dye sensitized solar cells by the use of conformally deposited metal oxide blocking layers. Journal of the American Chemical Society, 2003, 125(2): 475–482
8. Plank N O V, Howard I, Rao A, Wilson M W B, Ducati C, Mane R S, Bendall J S, Louca R R M, Greenham N C, Miura H, Friend R H, Snaith H J, Welland M E. Efficient ZnO nanowire solid-state dye-sensitized solar cells using organic dyes and core–shell nanostructures. Journal of Physical Chemistry C, 2009, 113(43): 18515–18522
9. Barea E, Xu X Q, Gonzalez-Pedro V, Ripollés-Sanchis T, Fabregat-Santiago F, Bisquert J. Origin of efficiency enhancement in Nb_2O_5 coated titanium dioxide nanorod based dye sensitized solar cells. Energy & Environmental Science, 2011, 4(9): 3414–3419
10. Ueno S, Fujihara S. Effect of an Nb_2O_5 nanolayer coating on ZnO electrodes in dye-sensitized solar cells. Electrochimica Acta, 2011, 56(7): 2906–2913
11. Yang M, Kim D, Jha H, Lee K, Paul J, Schmuki P. Nb doping of TiO_2 nanotubes for an enhanced efficiency of dye-sensitized solar cells. Chemical Communications (Cambridge, England), 2011, 47 (7): 2032–2034
12. Fiz R, Hernandez-Ramirez F, Fischer T, Lopez-Conesa L, Estrade S, Peiro F, Mathur S. Synthesis, characterization, and humidity detection properties of Nb_2O_5 nanorods and SnO_2/Nb_2O_5 heterostructures. Journal of Physical Chemistry C, 2013, 117(19): 10086–10094
13. Mäkinen V, Honkala K, Hakkinen H. Atomic layer deposition of aluminum oxide on TiO_2 and its impact on N3 dye adsorption from first principles. Journal of Physical Chemistry C, 2011, 115(18): 9250–9259
14. Lin C Y, Lai Y H, Chen H W, Chen J G, Kung C W, Vittal R, Ho K C. Highly efficient dye-sensitized solar cell with a ZnO nanosheet-based photoanode. Energy & Environmental Science, 2011, 4(9): 3448–3455
15. Zheng H D, Ou J Z, Strano M S, Kaner R B, Mitchell A, Kalantar-zadeh K. Nanostructured tungsten oxide – properties, synthesis, and applications. Advanced Functional Materials, 2011, 21(12): 2175–2196
16. Huang Y T, Cheng R, Zhai P, Lee H, Chang Y H, Feng S P. Solution-based synthesis of ultrasmall Nb_2O_5 nanoparticles for functional thin films in dye-sensitized and perovskite solar cells. Electrochimica Acta, 2017, 236: 131–139
17. Chu L, Liu W, Yu A, Qin Z F, Hu R Y, Shu H Z, Luo Q P, Min Y G, Yang J P, Li X A. Effect of TiO_2 modification on urchin-like orthorhombic Nb_2O_5 nanospheres as photoelectrodes in dye-sensitized solar cells. Solar Energy, 2017, 153: 584–589
18. Le Viet A, Jose R, Reddy M V, Chowdari B V R, Ramakrishna S. Nb_2O_5 photoelectrodes for dye-sensitized solar cells: choice of the polymorph. Journal of Physical Chemistry C, 2010, 114(49): 21795–21800
19. Sayama K, Sugihara H, Arakawa H. Photoelectrochemical properties of a porous Nb_2O_5 electrode sensitized by a ruthenium dye. Chemistry of Materials, 1998, 10(12): 3825–3832
20. Jia Z, Tang Y, Luo L, Li B, Chen Z, Wang J, Zheng H. Room temperature fabrication of single crystal nanotubes of $CaSn(OH)_6$ through sonochemical precipitation. Journal of Colloid and Interface Science, 2009, 334(2): 202–207
21. Fang X, Li Y, Zhang S, Bai L, Yuan N Y, Ding J N. The dye adsorption optimization of ZnO nanorod-based dye-sensitized solar cells. Solar Energy, 2014, 105: 14–19
22. Jo Y, Yun Y J, Alam Khan M, Jun Y. Densely packed setose ZnO nanorod arrays for dye sensitized solar cells. Synthetic Metals, 2014, 198: 137–141

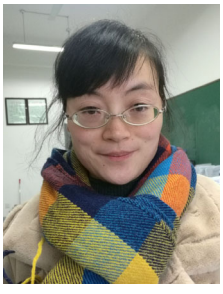

Xiaoyan Hu received her B.Sc, Master and Ph.D. degrees in 2008, 2010 and 2013 respectively from Center China Normal University, Wuhan, China. She is currently working at College of New Energy and Electronic Engineering, Yancheng Teachers University, China. Her research areas include nanomaterials and solar cells, particularly synthesizing one-dimensional ZnO by hydrothermal method.

Heng Wang received his B.Sc, Master and Ph.D. degrees in 2006, 2010 and 2013 respectively from Huazhong University of Science and Technology, Wuhan, China. He is currently working at College of New Energy and Electronic Engineering, Yancheng Teachers University, China. His research areas include dye-sensitized solar cells and perovskite solar cells, particularly solid-state dye-sensitized solar cells.